



HAL
open science

A two-dimensional analytical model of vertical water entry for asymmetric bodies with flow separation

Romain Hascoët, Nicolas Jacques, Yves-Marie Scolan, Alan Tassin

► To cite this version:

Romain Hascoët, Nicolas Jacques, Yves-Marie Scolan, Alan Tassin. A two-dimensional analytical model of vertical water entry for asymmetric bodies with flow separation. 2019. hal-02270373v2

HAL Id: hal-02270373

<https://hal.science/hal-02270373v2>

Preprint submitted on 19 Sep 2019

HAL is a multi-disciplinary open access archive for the deposit and dissemination of scientific research documents, whether they are published or not. The documents may come from teaching and research institutions in France or abroad, or from public or private research centers.

L'archive ouverte pluridisciplinaire **HAL**, est destinée au dépôt et à la diffusion de documents scientifiques de niveau recherche, publiés ou non, émanant des établissements d'enseignement et de recherche français ou étrangers, des laboratoires publics ou privés.

A two-dimensional analytical model of vertical water entry for asymmetric bodies with flow separation

Romain Hascoët^a, Nicolas Jacques^a, Yves-Marie Scolan^a, Alan Tassin^b

^a*ENSTA Bretagne, CNRS UMR 6027, IRDL, 2 rue François Verny, 29806 Brest Cedex 9, France*

^b*IFREMER – LCSM, ZI Pointe du Diable, 29280 Plouzané CS 10070, France*

Abstract

The vertical water entry of asymmetric two-dimensional bodies with flow separation is considered. As long as there is no flow separation, linearised Wagner’s theory combined with the Modified Logvinovich Model has been shown to provide computationally fast and reliable estimates of slamming loads during water entry. Tassin et al. (2014) introduced the Fictitious Body Continuation (FBC) concept as a way to extend the use of Wagner’s model to separated flow configurations, but they only considered symmetric bodies. In the present study, we investigate the ability of the FBC concept to provide accurate estimates of slamming loads for asymmetric bodies. In this case, flow separation may not occur simultaneously on both sides of the body. During an intermediate phase, slamming loads are governed by a competition between the local drop in pressure due to partial flow separation and the ongoing expansion of the wetted area. As a first benchmark for the model, we consider the water entry of an inclined flat plate and compare the FBC estimates with the results of a nonlinear model. Then, we consider the case of a foil and compare the FBC results with Computational Fluid Dynamics predictions. In both cases, we find that the FBC model is able to provide reliable estimates of the slamming loads.

Keywords: water entry, flow separation, Wagner’s model, cavity flow, Modified Logvinovich Model, NACA foil

1. Introduction

Water impacts are complex phenomena which have been extensively studied by means of experiments, analytical modelling and numerical simulations. From an engineering standpoint, it is crucial to know the hydrodynamic loads to which a body is exposed when entering water. Among the various applications, one can think of ship slamming, sloshing in tanks, aircraft ditching, water landing

*Corresponding author

Email address: `romain.hascoet@ensta-bretagne.fr` (Romain Hascoët)

of seaplanes. Experimental campaigns demand time and specific facilities, and protocols can face technical difficulties (e.g. pressure measurements). Modern Computational Fluid Dynamics (CFD) models offer hope for a detailed description of the impact-generated flow, but they are numerically demanding and the validation of results can be problematic; especially during the early stage of the impact. Alternatively, analytical developments require simplifying assumptions to make the problem tractable, but provide computationally fast results that are easier to check and control.

The pioneering work of Wagner (1932) [1] is still used as the basic framework of many (semi-)analytical models of water impact. One of the main approximations of Wagner’s model is the projection of the wetted body surface to the calm-water reference plane: the so called flat-disc or flat-plate approximation. Thus, Wagner’s approach is theoretically restricted to bodies with small deadrise angles. The flow is assumed to be potential and the speed of penetration is supposed sufficiently high to neglect gravity. In slamming problems, viscous effects can usually be considered negligible (e.g. [2]). The rapid expansion of the wetted area generates splash water jets at the line of contact which delimits the wetted surface of the body (hereafter the *contact line*) [3, 4]. These jets connect to the main flow through a root region where the curvature of the free surface is high and the flow is strongly nonlinear. Slamming pressure peaks in the root region, and quickly decreases toward the tip of the jet. Except for the root region, the water jets do not significantly contribute to the slamming loads [5]. Wagner’s problem is valid only if the wetted region is expanding [6]; i.e. there can be no migration of fluid particles from the wetted area to the free surface. Therefore, the classical Wagner model is not suitable to study water exit or the development of separated flows during water entry.

Flow separation may occur when the contact line reaches body knuckles, or smooth convex regions where the local deadrise angle reaches sufficiently large values. Then, a cavity flow forms behind the body and hydrodynamic loads usually start decreasing. It may be important to know how fast slamming pressure decays to predict the transient and vibratory response of the body structure. Besides, for asymmetric bodies or oblique entries, flow separation may not happen all at once over the contact line. Then there will be a transient phase where the evolution of slamming loads will be governed by a competition between the local drop in pressure due to flow separation and the ongoing expansion of wetted area. The water entry of finite wedges (flow separation at knuckles) has been extensively studied by means of experiments [7, 8, 9], analytical developments [10, 11, 12], fully nonlinear potential simulations [13, 14, 9, 15, 16], Navier-Stokes simulations [17, 18, 19] and smoothed-particle hydrodynamics method [20]. When flow separation occurs on a smooth part of the body, the location of the separation line is not known *a priori*, and it may evolve in time. The separation location can be sensitive to various parameters such as the impact velocity and the wettability properties of the body surface (see for example [21, 4, 22]). In hydrodynamic models of water entry, the microphysics of surface interactions – between water, air and the solid – is ignored. Flow separation on a smooth body is governed by pressure interaction between air and water at

the contact line (*nonviscous* separation), as illustrated by the CFD simulations of Zhu, Faltinsen and Hu (2006) [23]. When the fluid pressure in the jet root region drops below air pressure, air can seep in between the body and the main flow, leading to separation. Sun and Faltinsen (2006, 2007) [24, 25] used this criterion to trigger flow separation in a boundary element method (BEM) scheme and obtained good agreement with experiments on the separation location and the free surface of the early separated flow during the vertical water entry of a circular cylinder.

Inspired by the work of Logvinovich (1972) [10] and more recent publications [26, 27, 12], Tassin et al. (2014) [11] investigated the ‘Fictitious Body Continuation’ (FBC) concept as an effective way to extend the use of Wagner’s model after flow separation from the body. The principle of the FBC model is to extend the real body by a fictitious one so that Wagner’s model can be applied to the composite real+fictitious body. The pressure along the composite body contour is estimated by using the Modified Logvinovich Model (MLM), introduced by Korobkin (2004) [28]. Then, the hydrodynamic load is obtained by integrating the pressure along the real part of the body only. Within this approach, the main question to address is whether there exists a simple and generic fictitious body shape that can properly mimic the early expansion of the cavity flow behind the body. Tassin et al. [11] have given the first part of the answer by considering simple symmetric bodies: a horizontal flat plate, wedges with different deadrise angles and a circular cylinder. By comparing the FBC estimates with experimental and CFD results, they found that a continuation with inclined flat plates could give good agreements on the hydrodynamic loads during the early stage of cavity initiation. They found as ‘best-fit’ continuation angles, $\alpha \simeq 47^\circ$ for a flat plate, $\alpha \sim 45^\circ - 55^\circ$ for wedges with deadrise angles between 10° and 30° , and $\alpha \simeq 60^\circ$ for the circular cylinder. Interestingly, these continuation angles obtained for quite different shapes do not spread over a large range.

In the present paper, we go one step further and investigate whether the continuation by inclined flat plates can still provide satisfactory results for *asymmetric* bodies. Section 2 introduces the theoretical framework. In Section 3, we first consider the case of an inclined flat plate and compare FBC estimates with the nonlinear self-similar model of Faltinsen and Semenov (2008) [29]. In Section 4, we test the model capabilities on the vertical water entry of a foil, which is an asymmetric body mixing flow separations at a chine and on a smooth part of the body contour. FBC estimates are compared with CFD results obtained from simulations carried out with the finite-element software ABAQUS/Explicit. As FBC estimates are found to be reliable, we also give a qualitative and quantitative description of slamming loads on foils with different thicknesses. The model is further discussed in Section 5.

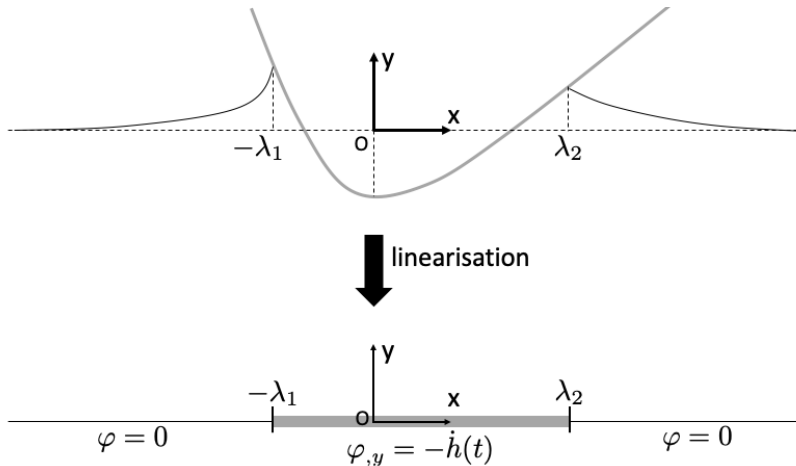


Figure 1: Illustration of Wagner’s model for vertical water entry. The boundary conditions are linearised and projected onto the initial free surface plane. The projection transforms the flow around the real body shape into the flow past a flat plate (both represented in grey). The size of the contact region is determined via the Wagner condition, which states that the vertical displacement is finite at $x = -\lambda_1, \lambda_2$.

2. Analytical model

2.1. Wagner’s model for a 2D asymmetric body

In Wagner’s model, the fluid is considered inviscid and incompressible. Gravity and surface tension effects are neglected (see appendix A for a discussion about the validity of the no gravity assumption). The flow is assumed to be irrotational, so the flow velocity \mathbf{V} can be expressed by the gradient of a scalar potential φ . Before its first contact with the body, the fluid is initially at rest and its domain is delimited by a flat free surface. The problem is formulated into a fixed coordinate system Oxy whose origin coincides with the location of the first fluid-body contact point (see Fig. 1). The body contour can be represented by a continuous shape function $f(x)$ satisfying $f(0) = 0$. At a given time, t , the location of the body contour is given by $y(x, t) = f(x) - h(t)$, where h is the vertical penetration depth of the body; h is positive and $h(0) = 0$. The local deadrise angle¹, $\beta(x) = \text{atan}(f_{,x}(x))$, between the body contour and the initial free surface is assumed to be small, $\beta \simeq f_{,x} \ll 1$. Following these assumptions, the mixed boundary value problem satisfied by the velocity potential can be linearised as follows (see Fig. 1 for illustration):

¹ In the present paper, $Q_{,v}$ denotes the derivative of the function Q with respect to the variable v .

$$\Delta\varphi = 0, \quad y < 0 \quad (1)$$

$$\varphi = 0, \quad y = 0, x \in]-\infty, -\lambda_1] \cup [\lambda_2, +\infty[\quad (2)$$

$$\varphi_{,y} = -\dot{h}(t), \quad y = 0, x \in]\lambda_1, \lambda_2[\quad (3)$$

$$\varphi \rightarrow 0, \quad x^2 + y^2 \rightarrow \infty \quad (4)$$

where \dot{h} is the time derivative of h (i.e. the vertical entry velocity). Eq. (1) is Laplace's equation restricted to the *initial* fluid domain. Eq. (2) is the linearised dynamic boundary condition of the free surface projected onto its initial plane. Eq. (3) is the impermeability condition expressed for the equivalent flat plate. Eq. (4) is the far-field condition. Although all equations are linearised and projected onto a fixed plane, the water entry problem remains nonlinear as the wetted region $[-\lambda_1, \lambda_2]$ is unknown *a priori*. The wetted area has to be determined together with the flow solution by imposing the so called Wagner condition at the fluid-body contact points

$$\eta(-\lambda_1, t) = f(-\lambda_1) - h(t), \quad (5)$$

$$\eta(\lambda_2, t) = f(\lambda_2) - h(t), \quad (6)$$

where $\eta(x, t)$ is the free surface elevation, and $h(t)$ the penetration depth. Using the linearised kinematic condition, the free-surface elevation is obtained from

$$\eta(x, t) = \int_0^t \varphi_{,y}(x, y = 0, \tau) d\tau, \quad (7)$$

which closes the problem. Eq. (1-7) form Wagner's problem.

By expressing Wagner's problem for the displacement potential

$$\Phi(x, y, t) = \int_0^t \varphi(x, y, \tau) d\tau, \quad (8)$$

and enforcing finite displacements at the contact points, Wagner's condition can be reduced to a system of two nonlinear equations (see [30] for details):

$$\int_{-\lambda_1}^{\lambda_2} f(x) \sqrt{\frac{\lambda_2 - x}{\lambda_1 + x}} dx = \frac{\pi}{2} (\lambda_1 + \lambda_2) h, \quad (9)$$

$$\int_{-\lambda_1}^{\lambda_2} f(x) \sqrt{\frac{\lambda_1 + x}{\lambda_2 - x}} dx = \frac{\pi}{2} (\lambda_1 + \lambda_2) h. \quad (10)$$

The penetration depth h enters Eqs. (9-10) as a parameter, which implies that the wetted area only depends on the current position of the body; the history of body kinematics has no influence. If $f(x)$ is a polynomial of low degree, the system of equations (9-10) can be analytically solved for λ_1 and λ_2 [31]. In the case of arbitrary shapes, these equations can be numerically solved by using a root-finding algorithm. In the present study, we use Newton's method with a relaxation condition (see appendix B for details).

2.2. Pressure

Knowing the expansion of the Wagner wetted area, the pressure can be computed by means of different models. The simplest one is the linearised Bernoulli equation

$$P(x, t) = -\rho\varphi_{,t}^{(w)}(x, 0, t), \quad (11)$$

where ρ is the fluid density and $\varphi^{(w)}$ is the velocity potential solution of Wagner's problem. For vertical water entry, $\varphi^{(w)}$ is the velocity potential on a flat plate:

$$\varphi^{(w)}(x, 0, t) = -\dot{h}(t)\sqrt{[\lambda_1(t) + x][\lambda_2(t) - x]}. \quad (12)$$

This linear model has been shown to overpredict hydrodynamics loads (see [32] for a detailed discussion). In order to improve pressure predictions, the quadratic term of Bernoulli's equation has to be taken into account. However, the quadratic term $[\varphi_{,x}^{(w)}]^2$ is not integrable at the contact points. To circumvent this difficulty, the Wagner flow solution can be asymptotically matched with a solution of the jet flow emerging from the root region [33, 5, 6, 34].

As an alternative, in the present work, we use the Modified Logvinovich Model (MLM), proposed more recently by Korobkin (2004) [28]. The MLM model takes into account the quadratic term and the shape of the body for the pressure calculation, by making use of the exact Bernoulli equation expressed at the body contour:

$$P(x, t) = -\rho \left[\phi_{,t} + \frac{f_{,x}\dot{h}}{1+f_{,x}^2}\phi_{,x} + \frac{1}{2(1+f_{,x}^2)}(\phi_{,x}^2 - \dot{h}^2) \right], \quad (13)$$

where P and ϕ are the pressure and the velocity potential along the body contour:

$$\begin{aligned} P(x, t) &= p(x, f(x) - h(t), t) \\ \phi(x, t) &= \varphi(x, f(x) - h(t), t). \end{aligned} \quad (14)$$

Then, the velocity potential ϕ is approximated by a first-order Taylor expansion of the Wagner solution, from the initial free surface level to the body height:

$$\phi(x, t) \simeq \varphi^{(w)}(x, 0, t) - \dot{h}(t)(f(x) - h(t)). \quad (15)$$

Thus part of the second order correction for the velocity potential is taken into account. Note however that the second-order perturbative component of the velocity potential is ignored in the MLM approach ; see [35, 36] for a second-order analysis of Wagner's model. Substituting Eq. (15) into Eq. (13), the MLM pressure for the vertical water entry of a 2D asymmetric body reads (see also [37]):

$$\begin{aligned} P(x, t) &= \underbrace{\frac{1}{2}\rho\dot{h}^2 \left[\frac{d\lambda_2}{dh} \sqrt{\frac{\lambda_1+x}{\lambda_2-x}} + \frac{d\lambda_1}{dh} \sqrt{\frac{\lambda_2-x}{\lambda_1+x}} - \frac{1}{4} \frac{(\lambda_2-\lambda_1-2x)^2}{(\lambda_2-x)(\lambda_1+x)(1+f_{,x}^2)} - 1 \right]}_{P_v(x,t)} \\ &\quad + \underbrace{\rho\ddot{h} \left[\sqrt{(\lambda_2-x)(\lambda_1+x)} + f(x) - h(t) \right]}_{P_a(x,t)}. \end{aligned} \quad (16)$$

The first and second terms of Eq. (16), P_v and P_a , respectively represent the slamming and added-mass pressures.

As the quadratic MLM pressure term ϕ_x^2 has non-integrable singularities close to the contact points, an additional condition has to be introduced to make the model effective. From an idea already expressed by Wagner [1], Korobkin [28] suggested to ignore regions of negative pressure close to the contact points. Negative pressure regions need to be ignored for the slamming term only, as the added-mass term is not singular at contact points.

Although this last condition lacks a physically grounded justification, the MLM model has shown good agreement with CFD simulations and experiments regarding the hydrodynamic force and the pressure distribution. The MLM model has been shown to be accurate up to relatively “large” deadrise angles (see [28, 37, 38]), beyond the original validity domain of Wagner’s model.

2.3. Fictitious Body Continuation

Tassin et al. [11] used the Fictitious Body Continuation concept to extend the use of Wagner’s model after flow separation from the body. Inspired by an original idea from Logvinovich (1972) [10], the principle of the FBC model is to extend the real body by a fictitious one so that Wagner’s model can be applied to the composite real+fictitious body. Then the hydrodynamic loads are obtained by integrating the MLM pressure along the real part of the body only. After flow separation, CFD simulations [39] indeed suggest that the hydrodynamic drag can still be decomposed into a velocity component proportional to \dot{h}^2 and an acceleration component proportional to \ddot{h} . As the added-mass pressure, P_a , is expected to level off after flow separation, Tassin et al. [11] modified the added-mass term of Eq. (16), as follows

$$P_a(x, t) = \rho \ddot{h} \left[f(x) - \min[h(t), f(l)] + \sqrt{\min(\lambda, l)^2 - x^2} \right], \quad (17)$$

for a symmetric body, where λ is the half-width of the wetted area on the composite body and $\pm l$ are the abscissa of the separation points. The presence of the minimum operators ensures that Eq. (17) is valid before and after flow separation. In the case of asymmetric bodies (see Fig. 4 for an illustration), this modification has to be generalised because separation does not occur at the same height and same time on both sides of the body. We suggest to use

$$P_a(x, t) = \rho \ddot{h} \left[f(x) - \min(h(t), \tilde{f}(x)) + \sqrt{(\min(\lambda_1, l_1) + x)(\min(\lambda_2, l_2) - x)} \right] \quad (18)$$

where $-l_1$ and l_2 are the abscissa of the separation points on the left and on the right respectively. When the flow separation occurs on a smooth part of the body, the location of the separation point depends on the shape chosen for the fictitious continuation (see §4.1 for the case study of a foil). \tilde{f} is a linear interpolation between the two separation heights

$$\tilde{f}(x) = f(-l_1) + \frac{x + l_1}{l_2 + l_1} [f(l_2) - f(-l_1)]. \quad (19)$$

In §4.3.3, we show that this simple prescription provides satisfactory agreement with CFD results.

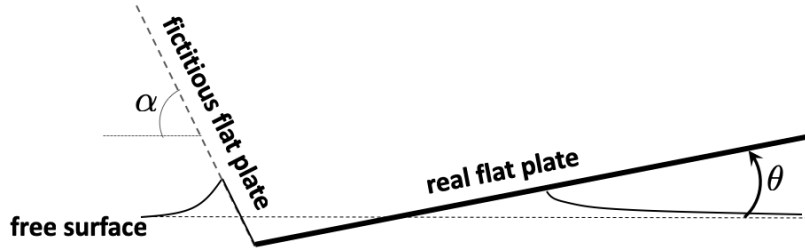


Figure 2: Vertical water entry of a flat plate – illustration. The flat plate is inclined by an angle θ . Flow separation on the left occurs right at the beginning of the water entry. In the FBC model the separated flow is mimicked by a fictitious flat plate with inclination α ; the real and fictitious flat plates form an inclined wedge.

3. Water entry of an inclined flat plate

3.1. Classical Wagner model with linearised Bernoulli equation

The vertical water entry of an inclined flat plate can be investigated with the classical Wagner model by assuming that the free surface of the separated flow expands vertically². Within the Fictitious Body Continuation concept, this corresponds to the situation where the real flat plate is continued from its leading edge by a vertical fictitious flat plate, with inclination angle $\alpha = 90^\circ$ (see Fig. 2). It is a limit case for Wagner’s model as the wetted area does not expand on one side of the body, leading to a singular free surface at the plate leading edge ($x = 0$). Thus the contact point location on the left is known *a priori*, $\lambda_1 = 0$, and the corresponding Wagner condition (Eq. 9) does not hold. The location of the other contact point is given by Eq. (10), setting $\lambda_1 = 0$:

$$\lambda_2^{(w)} = \frac{4}{3} \frac{h}{\tan \theta}. \quad (20)$$

Reinhard [40] obtained the same expression for $\lambda_2^{(w)}$ by using a slightly different approach: instead of imposing finite displacement at the contact point, he required the displacement potential to satisfy the far-field condition. For the sake of comparison (see the following paragraph), it is then interesting to give the resulting vertical force component obtained by integrating the linearised Bernoulli relation (Eq. 11):

$$\begin{aligned} F_y &= \frac{\pi}{4} \rho \dot{h} \lambda_2 \lambda_2 + \frac{\pi}{8} \rho \ddot{h} \lambda_2^2 \\ &= \frac{4\pi}{9} \frac{h}{\tan^2 \theta} \rho \dot{h}^2 + \frac{2\pi}{9} \frac{h^2}{\tan^2 \theta} \rho \ddot{h}. \end{aligned} \quad (21)$$

² In reality the separated flow free surface will expand in a more complicated shape; see for example [29].

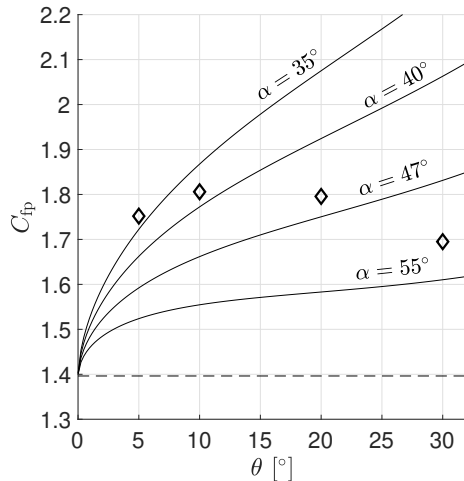


Figure 3: Vertical water entry of an inclined flat plate at constant velocity: normalised vertical force C_{fp} (see Eq. 22) as a function of the plate inclination angle θ . Solid lines show the predictions of the FBC model for different continuation angles α . The dashed line shows the prediction of the classical Wagner model with the use of linearised Bernoulli’s equation for pressure integration (Eq. 21). Diamonds show results from the nonlinear self-similar model of Faltinsen and Semenov [29].

3.2. Fictitious Body Continuation compared with a nonlinear model

The vertical force component acting on an inclined flat plate entering water can be normalised to a coefficient

$$C_{fp} = \frac{\tan^2 \theta}{h} \frac{F_y}{\rho h^2}, \quad (22)$$

where the factor $\tan^2 \theta$ has been added to limit the range of values. Flow separation occurs at the leading edge, right at the first fluid-solid contact. This configuration can be addressed with the FBC model by connecting a fictitious flat plate to the leading edge of the real flat plate (see Fig. 2). Within this framework, the flow induced by the inclined flat plate is self-similar and C_{fp} does not depend on the penetration depth h if the entry velocity is constant.

Fig. 3 shows the force coefficient C_{fp} predicted by the FBC model, as a function of the plate inclination angle θ , for constant entry velocity. Estimates are plotted for different continuation angles of the fictitious flat plate. To assess the relevancy of the FBC concept, our results are compared with calculations from the nonlinear self-similar model of Faltinsen and Semenov (see Table 2 in [29]). For a continuation angle $\alpha = 47^\circ$, both models agree by $\sim 10\%$ over a range of inclination angles $\theta = 5^\circ \rightarrow 30^\circ$. This is consistent with the results obtained by Tassin et al. (2014) [11] for the vertical water entry of a horizontal flat plate: by comparing with the numerical calculations of Iafrati and Korobkin (2008) [41], they found that the FBC model with $\alpha = 47^\circ$ can reproduce the early decay of the hydrodynamic force acting on the plate. The force coefficient

| | w | R_0/c | δ [°] | θ_s [°] | θ_m [°] | R_m/c |
|-----------|------|----------------------|--------------|----------------|----------------|---------|
| NACA 0005 | 0.05 | $2.76 \cdot 10^{-3}$ | 3.35 | -0.71 | -2.59 | 18.1 |
| NACA 0010 | 0.1 | $1.10 \cdot 10^{-2}$ | 6.67 | -1.5 | -5.19 | 9.14 |
| NACA 0020 | 0.2 | $4.41 \cdot 10^{-2}$ | 13.2 | -3.2 | -10.4 | 4.74 |
| NACA 0028 | 0.28 | $8.64 \cdot 10^{-2}$ | 18.1 | -4.9 | -14.5 | 3.55 |
| NACA 0030 | 0.3 | $9.92 \cdot 10^{-2}$ | 19.3 | -5.5 | -15.5 | 3.36 |

Table 1: Some properties of the NACA foils considered in the present study. w is the maximum thickness, normalised by the chord length c . R_0 is the radius of curvature at the leading edge. δ is the half-opening angle of the trailing edge. θ_s is the inclination angle for which flow separation is simultaneous at the leading and trailing edges, within the FBC model. R_m is the maximum radius of curvature along the foil contour. θ_m is the inclination angle for which the first fluid-body contact occurs at the point where the radius of curvature is maximum.

C_{fp} predicted by the nonlinear model of Faltinsen and Semenov starts decreasing for $\theta \gtrsim 20^\circ$, while the values obtained from the FBC model with $\alpha = 47^\circ$ keep increasing. In principle, it should be possible to find a “phenomenological” law $\alpha(\theta)$ for which agreement between both models remains good for $\theta \gtrsim 30^\circ$. We do not attempt to give such a law in the present paper.

For $\theta \rightarrow 0$, all FBC curves converge to the same coefficient value $C_{fp} \simeq 1.4$. This asymptotic value coincides with the force coefficient predicted by the classical Wagner model, $C_{fp} = 4\pi/9$ (see Eq. 21). This can be understood as follows. First as $\theta \rightarrow 0$, the wetted area on the real plate expands much faster than on the fictitious one, with $\lambda_1/\lambda_2 \rightarrow 0$, resulting in $\lambda_2 \rightarrow \lambda_2^{(w)}$. Then, an asymptotic analysis of Eq. (16), at a given self-similar abscissa x/λ_2 , shows that the MLM pressure tends to the linearised Bernoulli pressure as $d\lambda_2/dh \rightarrow +\infty$.

4. Vertical water entry of a foil

4.1. NACA foil: geometry, flow separation, and choice of continuation angles

In this paragraph, we go one step further by considering the vertical water entry of a NACA³ foil [42]. The half-thickness of a symmetric NACA foil is given by

$$g(\xi) = c \cdot \frac{w}{0.2} \left[0.2969 \sqrt{\frac{\xi}{c}} - 0.1260 \left(\frac{\xi}{c}\right) - 0.3516 \left(\frac{\xi}{c}\right)^2 + 0.2843 \left(\frac{\xi}{c}\right)^3 - 0.1015 \left(\frac{\xi}{c}\right)^4 \right], \quad (23)$$

where c is the chord length, $c \cdot w$ is the maximum thickness and ξ is the position along the chord ($\xi = 0$ at the leading edge, $\xi = c$ at the trailing edge). The leading edge of the foil approximates a circular cylinder of radius

$$R_0 \simeq 1.102w^2c, \quad (24)$$

³ The National Advisory Committee for Aeronautics (NACA) was a US federal agency, replaced with the National Aeronautics and Space Administration (NASA) in 1958.

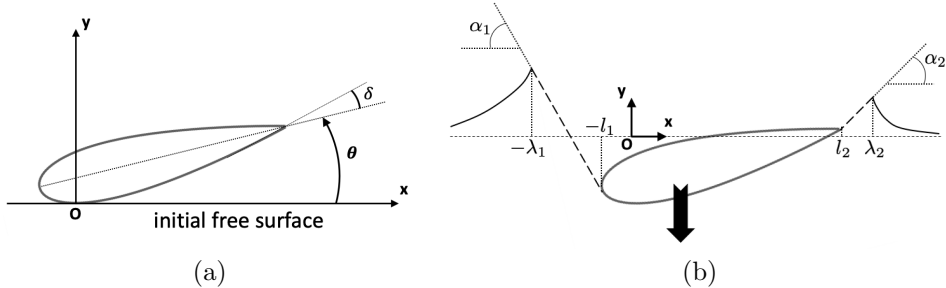


Figure 4: (a): Initial conditions of impact when the foil first touches the water. The initial free surface is assumed to be flat; θ is the inclination angle of the foil with respect to the initial free surface; δ is the half opening angle of the trailing edge. (b): Fictitious body continuation after flow separation from both sides of the foil. The foil is continued by two flat plates (dashed lines) of inclinations, α_1 on the left, and α_2 on the right.

and the half opening angle of the trailing edge is given by

$$\delta = \text{atan}(1.169 w). \quad (25)$$

In §4.3, we consider a NACA 0028 foil, whose contour follows Eq. (23) with $w = 0.28$ (see Fig. 4 for illustration). NACA foils with other thicknesses are considered in §4.4; some characteristics of the foils considered in the present paper are given in Tab. 1.

During the water entry of a foil, flow separation can occur on both sides of the body, requiring the choice of two continuation angles α_1 and α_2 within the FBC framework (see Fig. 4). At the foil leading edge, a tangential connection between the real body and the fictitious sloped plate is imposed; thus, the choice of α_1 also sets the connection point between the fictitious plate and the foil leading edge. Then, the flow separation takes place at the point of the body contour where the local deadrise angle is equal to α_1 . This tangential connection is motivated by experiments and numerical results, which show that the flow separation from a smooth body leads to a smooth transition in terms of the hydrodynamic force. In principle, the continuation angles α_1 and α_2 could be functions of θ . In the present paper, we investigate to what extent the choice of α_1 and α_2 can be generic, and set the values, only depending on the type of separation:

1. At the leading edge, flow separation occurs on a smooth part of the contour. In this case we set $\alpha_1 = 60^\circ$, which is the continuation angle obtained by Tassin et al. (2014) [11] for a circular cylinder.
2. Close to the trailing edge, the radius of curvature of the contour becomes large, and separation occurs at a chine. Therefore we set $\alpha_2 = 47^\circ$, which is the continuation angle recommended by Tassin et al. (2014) [11] for a horizontal flat plate. This choice is also consistent with the results obtained in Section 3 for the water entry of an inclined flat plate.

4.2. CFD simulations

In order to have a point of comparison and assess the applicability of the FBC concept to a foil shape, the same water entry configurations were investigated by means of Computation Fluid Dynamics. The simulations have been carried out with the finite-element software ABAQUS/Explicit (version 2017), using the coupled Eulerian-Lagrangian formulation. In this framework, the impacting body is modelled as a Lagrangian solid (rigid in the present case), while the fluid flow is described using the Eulerian approach. The position of the fluid surface is tracked using the Volume-Of-Fluid (VOF) method, coupled with an interface-reconstruction scheme. As viscosity does not play a significant role in water impact problems, it is not considered in the present simulations. Accounting for viscosity would have required a very fine mesh, to properly resolve the boundary layer. The purpose of these simulations is to validate the FBC concept, therefore gravity is not included. The general contact algorithm of ABAQUS is used to describe the interaction between the fluid and the solid. In this method, only compressive stresses are transmitted across the fluid-solid interface, and flow separation occurs when the pressure on the body contour drops to zero.

As the ABAQUS/Explicit solver is not able to deal with incompressible flows, fluid compressibility was taken into account. For the impact of a *blunt* body, compressibility matters only at the very beginning of water entry. At small penetration depths, a blunt body contour approximates a parabola and the expansion velocity of the Wagner wetted area follows

$$\dot{\lambda}_1 \simeq \dot{\lambda}_2 \simeq \sqrt{\frac{R_c}{h}} \dot{h}, \quad \text{for } h \rightarrow 0, \quad (26)$$

where R_c is the radius of curvature of the body contour at the point of first contact with the fluid. The typical penetration depth, over which fluid compressibility matters (see for example [43]), can be obtained by equating the expansion velocity of the Wagner wetted surface with the speed of sound in the liquid, c_l :

$$h_c = \left(\frac{\dot{h}}{c_l} \right)^2 R_c. \quad (27)$$

In the CFD simulations reported hereafter, the impacting solid is a NACA 0028 foil with a chord length $c = 1$ m and a velocity at first contact with water, $\dot{h} = 1$ m/s (except for one simulation reported in §4.3.3, where the solid body starts at rest). The speed of sound is set to $c_l = 500$ m/s and the maximum radius of curvature along the foil contour is 3.5 m, leading to $h_c \simeq 1.4 \cdot 10^{-5}$ m. This value is much smaller than the penetration depths relevant to slamming loads (see Figs. 6-7).

The Eulerian fluid domain is 20 m in width and 10 m in height. Non-reflecting boundary conditions are enforced at the remote boundaries of the fluid domain to minimise the reflection of acoustic waves. Two different meshes have been considered. The first mesh features 347733 elements with a mesh spacing of $\Delta x = 5$ mm in the region where the fluid-solid interaction takes place. The

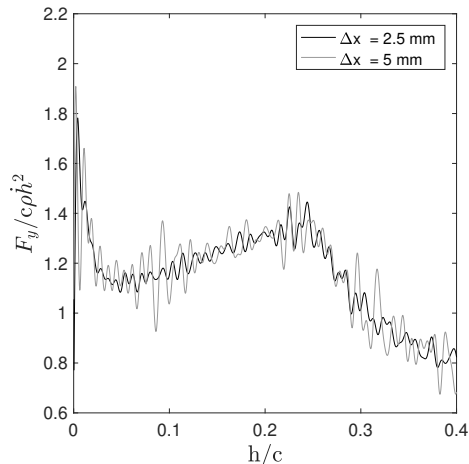


Figure 5: The effect of mesh resolution on ABAQUS simulations. The quantity shown is the nondimensional vertical force component as a function of the nondimensional penetration depth, for the water entry of a NACA 0028 foil at constant velocity $\dot{h} = 1$ m/s, with an inclination angle $\theta = 20^\circ$. CFD results are shown for two different grid spacings: $\Delta x = 5$ mm (grey curve) and $\Delta x = 2.5$ mm (black curve).

second mesh features 703800 elements with a mesh spacing in the impact area of $\Delta x = 2.5$ mm. Fig. 5 shows the evolution of the vertical component of the hydrodynamic force obtained with the two meshes, for the vertical water entry of a NACA 0028 foil at constant velocity. Both curves show some high-frequency oscillations. These oscillations are probably due to the Euler-Lagrange contact algorithm, which is based on a penalty method [44]. In a previous study [45], the present CFD solver has been shown to provide accurate estimates of slamming loads for various body shapes. When the mesh is refined, the magnitude of the oscillations is reduced. However, the overall force evolution remains unchanged. All results presented in the rest of the present paper have been obtained with the finest mesh ($\Delta x = 2.5$ mm).

4.3. Comparison of the analytical model with CFD results

Figs. 6-7 show the evolution of the two hydrodynamic force components F_x , F_y , and of the moment M_z (expressed at the foil leading edge) acting on a NACA 0028 foil, during vertical water entry at constant velocity. The FBC predictions are compared with the CFD results for 5 different inclination angles: $\theta = -28.1^\circ$; -18.1° ; -14.5° ; 0° ; 20° . Fig. 8 shows two additional comparisons for water entries at constant acceleration.

The results reported in this section are nondimensionalized and given in terms of hydrodynamic coefficients. Semi-analytical results were directly computed in a dimensionless form. Regarding CFD simulations, for the water entries at constant velocity, a specific value of the velocity, $\dot{h} = 1$ m/s, had to be specified. As long as the fluid viscosity, surface tension, flow compressibility, and

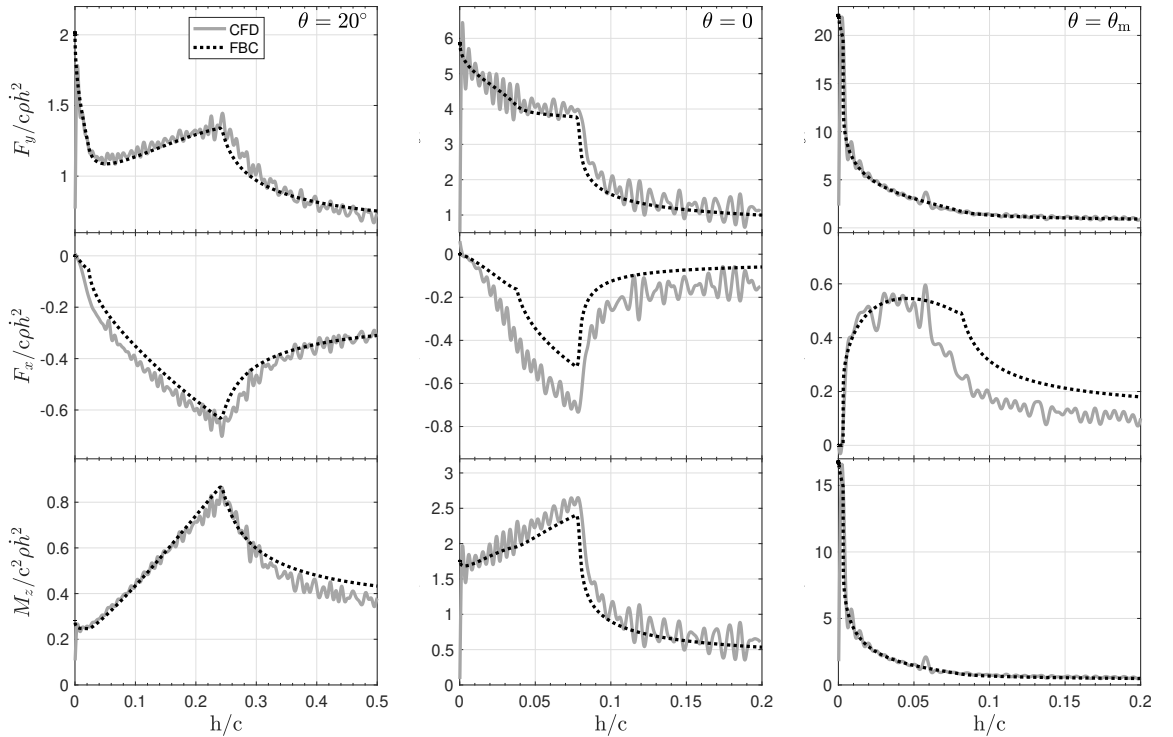


Figure 6: Vertical water entry of a NACA 0028 foil at constant velocity. CFD and FBC results are shown respectively as grey solid lines and black dotted lines. From top to bottom: normalised force components and moment, F_y , F_x , M_z . From left to right: calculations are shown for different inclination angles, $\theta = 20^\circ$ (left), $\theta = 0$ (middle), $\theta = \theta_m$ (right). $\theta_m = -14.5^\circ$ is the inclination angle at which the FBC model predicts maximum instant value for $F_y/c\dot{h}^2$ (at the beginning of the impact).

gravity effect can be neglected, the chosen value of the velocity is expected to have no effect on the slamming coefficients reported in Figs. 6-7. For the water entries at constant acceleration, an acceleration, \ddot{h} , and an initial velocity, $\dot{h}(0)$, had to be specified. In these cases, an added-mass load adds to the slamming load (see Eq. 16). A rescaling of the chord length and body kinematics keeping the ratio $\dot{h}(0)^2/c\ddot{h}$ unchanged would have no effect on the hydrodynamic coefficients reported in Fig. 8, as long as the same above-mentioned assumptions are valid. In the following paragraphs, we discuss several aspects of our results.

4.3.1. Times of flow separation

For $\theta = 0^\circ; 20^\circ$, the flow separation first occurs at the leading edge and then at the trailing edge. For $\theta = -28.1^\circ; -18.1^\circ; -14.5^\circ$, the flow separation sequence is reversed. For $\theta = -28.1^\circ; -18.1^\circ$, the flow separates from the trailing edge right at the first fluid-body contact. Flow separation events can be easily

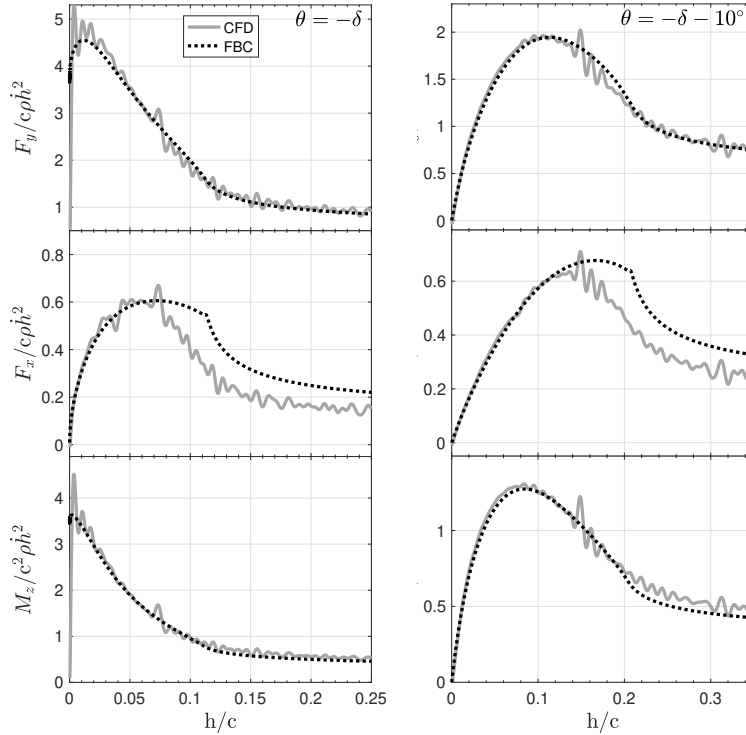


Figure 7: Same as Fig. 6 for two other inclination angles: $\theta = -\delta$ (left) and $\theta = -\delta - 10^\circ$ (right). $\delta \simeq 18.1^\circ$ is the half opening angle of the foil trailing edge (see Eq. 25). For $\theta = -\delta$ the trailing edge contour is tangent to the initial free surface.

identified for the FBC model as they induce discontinuities in the slope of the force-displacement curves. Flow separation transitions can also be identified in CFD results at the same penetration depths, although they are somewhat smoothed in some of the F_x curves. For all inclination angles, both models show a good agreement on separation times.

4.3.2. Force components F_x , F_y and moment M_z

The FBC and CFD models agree very well in terms of vertical force F_y and moment M_z , for all considered inclination angles. The agreement is less satisfactory regarding the horizontal force component F_x (except for $\theta = 20^\circ$). We note, however, that the magnitude of F_x is significantly smaller than the magnitude of F_y for the considered range of inclination angles. This larger disagreement is not surprising since F_x , given by (see §2.3 for an explanation about the limits of integration)

$$F_x(t) = - \int_{-\min(\lambda_1, l_1)}^{\min(\lambda_2, l_2)} P(x, t) f_{,x}(x) dx, \quad (28)$$

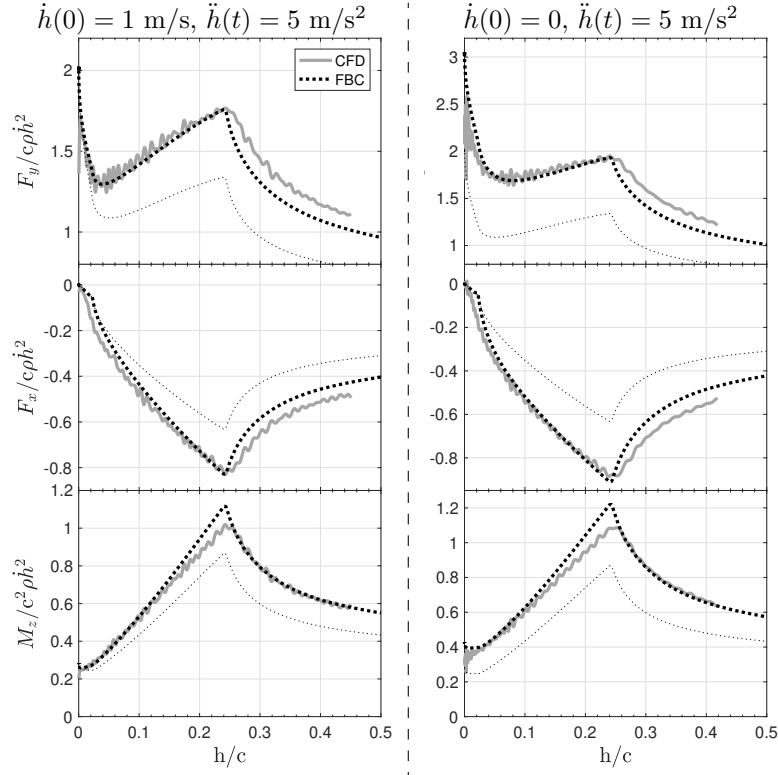


Figure 8: Vertical water entry of a NACA 0028 foil (chord length, $c = 1$ m) at constant acceleration, $\ddot{h}(t) = 5$ m/s². CFD and FBC results are shown respectively as grey lines and black dotted lines. From top to bottom: normalised force components and moment, F_y , F_x , M_z . Calculations are shown for 2 different initial velocities (at first contact with the fluid): $\dot{h}(0) = 1$ m/s (left) and $\dot{h}(0) = 0$ (right). For comparison purpose, FBC results with no acceleration (same curves as in Fig. 6, left panel) are shown as thin dotted lines.

is a second-order quantity whose main contributions are concentrated close to the contact points. Indeed, the splash root is the region where the pressure *and* the deadrise angles (i.e. $f_{,x}$) are the largest for a curved contour. Thus, the integral in Eq. (28) is largely dominated by regions where the flow nonlinearities, ignored in Wagner’s approach, are the strongest. This explains why the MLM estimates for F_x are not as reliable as for F_y and M_z . For practical use, it is not an issue as long as F_x remains moderately smaller than F_y . This last condition is guaranteed for body contours with moderate deadrise angles ($\lesssim 30^\circ$), or body contours which are not strongly asymmetric.

4.3.3. Water entry with acceleration

Fig. 8 shows two examples of the simulated slamming load evolution when the foil impacts water at constant acceleration. The foil is inclined at an angle

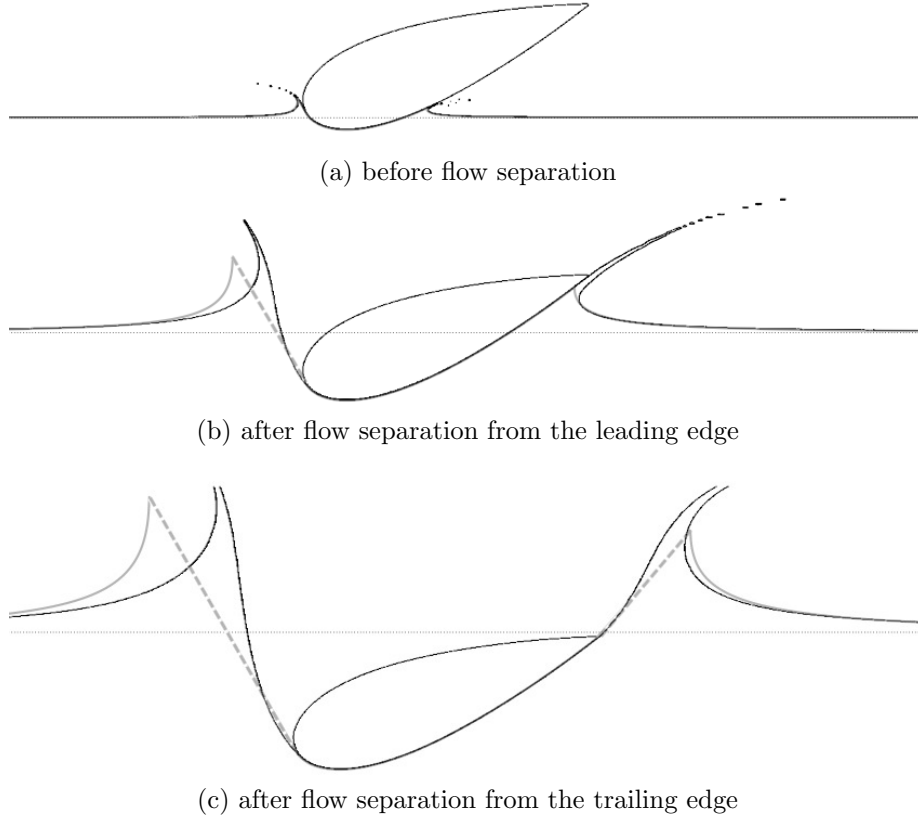


Figure 9: Free surface of the flow induced by the vertical water entry of a NACA 0028 foil. The inclination angle is $\theta = 20^\circ$ and the entry velocity is constant, $\dot{h} = 1$ m/s. The free surface extracted from CFD simulations (black line) is compared with the fictitious flat plates (dashed grey lines) and the free surface (solid grey lines) obtained from the FBC model. The initial free surface is shown as a thin dotted line. Snapshots are given for 3 different penetration depths: (a) $h/c = 0.041$, (b) $h/c = 0.23$, (c) $h/c = 0.43$.

$\theta = 20^\circ$ and is accelerated into the fluid at $\ddot{h}(t) = 5$ m/s². At first contact with the fluid two different initial velocities are considered: $\dot{h}(0) = 0$ and $\dot{h}(0) = 1$ m/s. The results obtained with the FBC approach for constant velocity are also depicted in Fig. 8 for the sake of comparison. As the velocity used for the normalisation of F_y is the *instantaneous* velocity, the comparison with the curves obtained for constant velocity directly reflects the contribution of the added-mass force. The FBC model predicts a slightly faster decay of the force after flow separation from the trailing edge and a larger peak value of M_z (by $\simeq 10\%$), compared to the CFD results. Still, the FBC model gives a good estimate of the added mass loads during the early stage of flow separation.

4.3.4. Free surface

Fig. 9 shows three snapshots of the free surface, taken during the water entry of the foil inclined at an angle $\theta = 20^\circ$, with constant velocity. The free surface profile extracted from the CFD simulations (black line) is compared with the fictitious flat plates and free surface elevation obtained from the FBC model (grey line). Before flow separation (Fig.9-a), the agreement between the CFD and Wagner models is excellent.

After flow separation from the leading edge, the FBC free surface rapidly deviates from the CFD free surface (Fig.9-b). However, on the other side of the body (trailing edge), the flow has not separated yet. One can note the prominent water jet that has formed in the CFD simulation, and which is disregarded in Wagner’s model. As mentioned in the introduction, the splash jets do not contribute significantly to the hydrodynamic loads. Except for the jet, both models show a good agreement on the expansion rate of the wetted surface towards the trailing edge. This explains why the FBC model still provides satisfactory load estimates after flow separation from the leading edge.

After flow separation from both sides of the foil (Fig.9-c), the FBC free surface elevation on the trailing edge side also starts deviating from the CFD shape. Then it becomes more difficult to qualitatively explain why the agreement on predicted hydrodynamic loads remains good (see Fig. 6).

4.4. Slamming loads on foils of different thicknesses

Using CFD results for comparison, the FBC concept has been shown to provide reliable estimates of the slamming loads on a NACA 0028 foil. The present paragraph gives a more systematic description of the slamming loads acting on foils entering water, based on FBC estimates only. Figs. 10-11 show the evolution of slamming loads as a function of the penetration depth h and inclination angle θ for NACA foils of different thicknesses. The inclination angle θ is restricted to $-30^\circ \rightarrow 20^\circ$, range for which the FBC results have been compared to the CFD simulations in §4.3. As the FBC estimates for F_x have been found to be not as reliable as for F_y and M_z , they are not shown in Figs. 10-11. This is not an issue for discussion purpose, since the magnitude of F_x is much smaller than the magnitude of F_y .

4.4.1. Initial slamming loads

If the first contact occurs at a blunt point, the body contour can be locally approximated by a parabola $f(x) = x^2/2R_c$, where R_c is the local radius of curvature. The half-width of the wetted region for a parabola is given by $\lambda = 2\sqrt{hR_c}$. When $h \rightarrow 0$ the expansion rate of the wetted correction becomes infinite: the MLM pressure reduces to linearised Bernoulli’s relation (same argument as in §3.1), and the added-mass pressure becomes negligible. This results

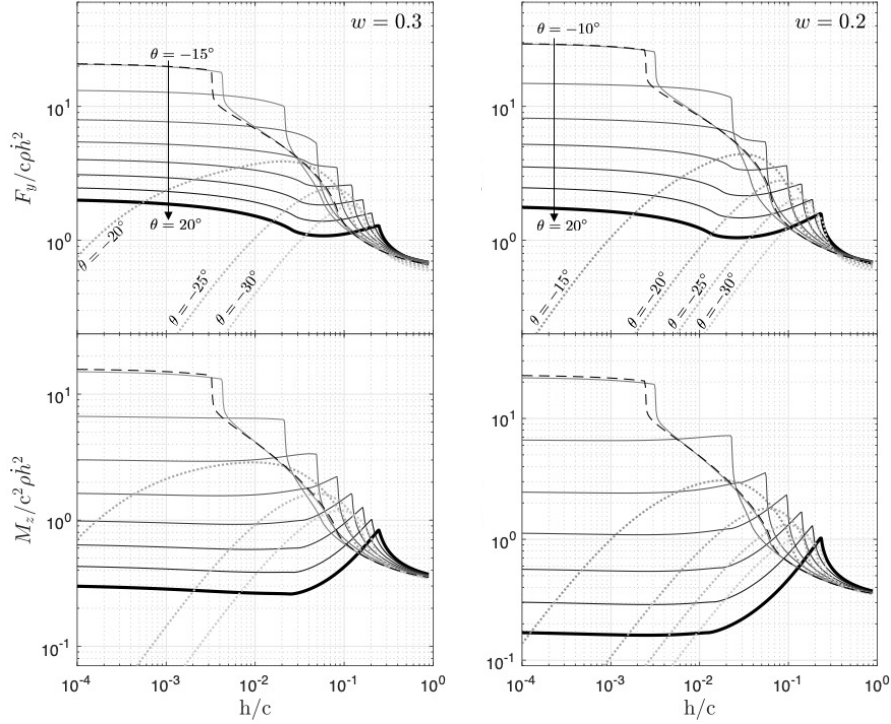


Figure 10: Slamming loads on foils during a vertical water entry at constant velocity. The evolution of the nondimensional vertical force component $F_y/c\rho\dot{h}^2$ and the nondimensional moment $M_z/c^2\rho\dot{h}^2$ (computed at the foil leading edge) are given as a function of the nondimensional penetration depth h/c . Results are shown for two relative foil thicknesses (see Eq. 23): $w = 0.3$ (left) and $w = 0.2$ (right). The slamming loads are plotted for different inclination angles using a gradation of grey, from $\theta = -30^\circ$ (light grey) to 20° (black) with a 5° -step between two successive curves. To ease the reading, dotted lines are used when the first contact with the fluid occurs at the trailing edge ($\theta < -\delta$, see Tab. 4), and the curve for $\theta = 20^\circ$ is thickened. The dashed black lines show the slamming loads obtained for the inclination angle θ_m (see Tab. 4), which gives the maximum instant loads (at first contact with the fluid).

in the following asymptotic value⁴ of F_y

$$\lim_{h \rightarrow 0} \frac{F_y(h)}{\rho\dot{h}^2} = \frac{F_y(0)}{\rho\dot{h}^2} = 2\pi R_c. \quad (29)$$

⁴ The asymptotic value is different for a body initially at rest on the free surface, suddenly accelerating into the fluid. In this case, added-mass pressure is not negligible and one can show that $\lim_{h \rightarrow 0} \frac{F_y(h)}{\rho\dot{h}^2} = 3\pi R_c$. As an illustration, see Fig. 8 and compare initial values of $F_y/\rho\dot{h}^2$ on left and right panels.

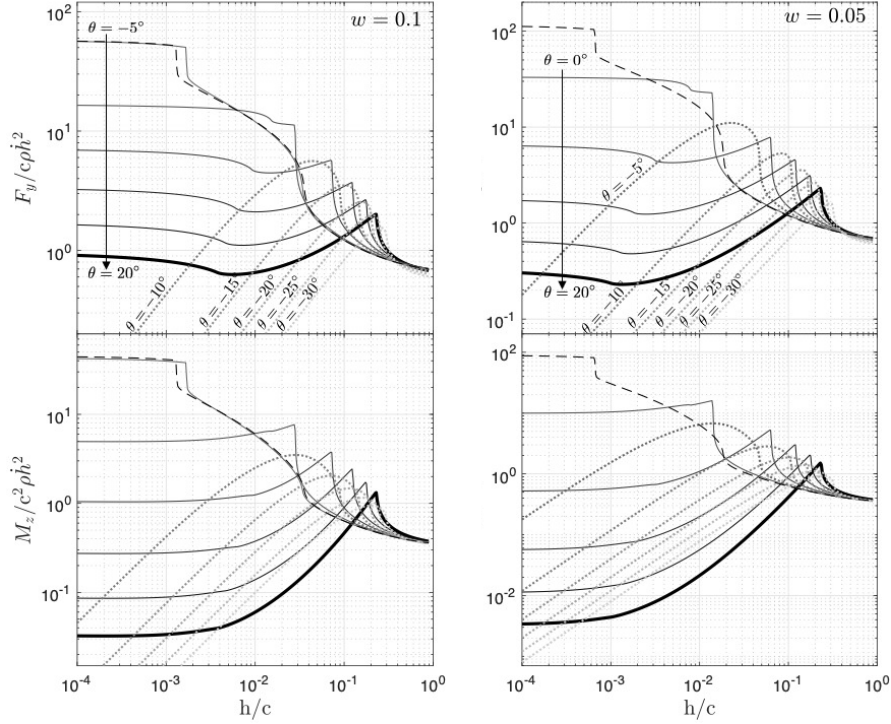


Figure 11: Same as Fig. 10 for different foil thicknesses: $w = 0.1$ (left) and $w = 0.05$ (right).

In Figs. 10-11, all the F_y curves for $\theta > -\delta$ converge towards the asymptotic value given by Eq. (29). For $\theta < -\delta$, the first contact with the fluid occurs at the sharp trailing edge and $F_y(0) = 0$. For a given foil thickness, the maximum values of R_c and $F_y(0)/\rho h^2$ are obtained for a negative inclination angle $\theta = \theta_m$ (values are given in Tab. 1). The slamming loads for $\theta = \theta_m$ are shown as dashed black lines in Figs. 10-11.

4.4.2. Time evolution of the slamming loads and flow separation

For $\theta = 20^\circ$, flow separation first occurs at the leading edge and then at the trailing edge. Starting from an initial value given by Eq. (29), F_y decreases and reaches a local minimum. Then, F_y starts rising as the wetted area on the foil keeps increasing towards the trailing edge. When the flow separates from the trailing edge, F_y reaches a peak at $h/c \simeq 0.2 - 0.3$ and starts decreasing again. These peak values are local maxima for $w = 0.3; 0.2$, and global maxima for $w = 0.1; 0.05$. Conversely, flow separation from the leading edge does not induce a sudden change of slope in the evolution of F_y and M_z , as it occurs on a smooth part of the body.

Then as θ decreases from 20° to -30° , separation at the leading edge and

the trailing edge happen respectively later and earlier. Separation happens simultaneously on both sides for a negative value of inclination angle, $\theta = \theta_s$ (values are given in Tab. 1). For $-\delta < \theta < \theta_s$, the separation from the trailing edge induces a sharp drop in F_y and M_z , whereas the separation from the leading edge still does not induce a sharp transition.

For $\theta < -\delta$, first contact with the fluid occurs at the trailing edge. At early times, the wetted contour of the foil locally resembles an inclined flat plate; F_y linearly increases with h . As the fluid-body contact point approaches the leading edge, the deadrise angles increase resulting in a lower increase rate of F_y ; the vertical force F_y starts decreasing slightly before the flow separation from the leading edge.

5. Discussion

We have shown that the Fictitious Body Continuation concept can be effectively used to estimate the hydrodynamic loads during the vertical water entry of two-dimensional asymmetric bodies, including flow separation. The FBC method is computationally fast and simple to implement compared to CFD or BEM methods. Although the FBC model can properly mimic flow separation regarding hydrodynamic loads on the body, we note that it does not provide a proper description of the free surface shape after flow separation.

In the present study, the real body contour is continued by fictitious flat plates. Then the critical point in the model is the choice, *a priori*, of the continuation angles α_1 and α_2 . Comparisons with experiments or self-sufficient models (e.g. CFD simulations) are required to have some ‘heuristic’ knowledge of suitable continuation angles. This question was partly investigated by Tassin et al. (2014) [11], considering simple symmetric body shapes. They found as ‘best’ continuation angles, $\alpha_{fp} = 47^\circ$ for a horizontal flat-plate, $\alpha_{cl} = 60^\circ$ for a circular cylinder, and $45^\circ - 55^\circ$ for wedges with different deadrise angles. For more general asymmetric bodies, one practical way of using the FBC concept could be to find the appropriate ‘phenomenological’ laws for continuation angles as a function of body orientation, α_1 and α_2 . Such laws could be derived from the interpolation (or regression) of best-fit values obtained through comparisons with experiments or CFD simulations carried out for a few inclination angles.

However, the present work shows that best continuation angles may weakly depend on the exact shape of the real body contour. In Section 3, we have found that the continuation angle α_{fp} is suitable to mimic the separated flow emerging from the tip of an inclined flat plate up to $\theta \simeq 30^\circ$. In this range of inclination angles, the FBC results agree with the nonlinear model of Faltinsen and Semenov [29] by 10%. In Section 4, we have considered the vertical water entry of a foil, as a more complicated body shape. We have set the continuation angles to $\alpha_1 = \alpha_{cl}$ for flow separation at the smooth leading edge, and $\alpha_2 = \alpha_{fp}$ at the sharp trailing edge. Through comparisons with CFD simulations, we have shown that the FBC model provides good estimates of the slamming loads on the foil for a broad range of inclination angles ($-30^\circ < \theta < 20^\circ$); this, without any change in the values of α_1 and α_2 . From these encouraging results, one

could wonder whether α_{fp} and α_{cl} – for flow separation at a chine and from a smooth body part respectively – can be used as generic continuation angles for a broad family of body shapes. Comparative studies for other asymmetric bodies would be useful to better delimit the generic feature of continuation angles.

Acknowledgements

This work was supported by the French National Agency for Research (ANR) and the French Government Defense procurement and technology agency (DGA) [ANR-17-ASTR-0026 APPHY].

Appendix A. No gravity assumption: limit of validity

In Wagner’s approach, the effect of gravity on the flow dynamics is neglected. To assess the validity of this assumption, for a given configuration of water entry, the acceleration of the liquid can be compared with the gravitational acceleration. For the sake of simplicity, let us consider the case of a symmetric body ($\dot{\lambda}_1 = \dot{\lambda}_2 = \dot{\lambda}$), entering water at constant velocity. Then, the acceleration field of the fluid, deriving from the velocity potential $\varphi^{(w)}$ (Eq. 12), is given by

$$\varphi_{,xt}^{(w)}(x, 0, t) = -\dot{h} \frac{\dot{\lambda}}{\lambda} \frac{x/\lambda}{[1 - (x/\lambda)^2]^{3/2}}. \quad (30)$$

In Wagner’s approach, the deadrise angle is assumed to be small, $\beta \ll 1$, and the convective acceleration can be neglected to the leading order. Besides, the only force considered in the fluid domain is the one due to the pressure gradient: Eq. (30) can also be obtained by considering the pressure force density $-\nabla P/\rho$, from the linearised Bernoulli relation (Eq. 11).

In Eq. (30), the quantity

$$\dot{h} \frac{\dot{\lambda}}{\lambda} \sim \frac{\dot{h}^2}{h} = \frac{\dot{h}}{t} \quad (31)$$

appears as the relevant scale for the fluid acceleration. Then, gravity can be neglected if $\dot{h}/t \gg \beta g$, leading to the constraint

$$t \ll t_g = \frac{\dot{h}}{\beta g}. \quad (32)$$

The factor $1/\beta$ accounts for the fact that only the gravity component acting along streamlines (on the body surface) should be considered. After flow separation from the body, the situation is different as the separated flow (especially jets) is “free” to plunge and can impact on the underlying liquid surface. Besides, the cavity flow can begin to collapse; see Bao et al. [15] for BEM simulations of the water entry of a finite wedge at different velocities. Then, it may be safer to consider Eq. (32) without the factor $1/\beta$.

To our knowledge, few studies did a systematic study of gravity effect in the water entry problem. The pioneering work of Mackie [46] was maybe the first to focus on the effect of gravity in the water entry problem. However, his analytical developments make the assumption of very large deadrise angles (β close to 90°); i.e. the extreme opposite of Wagner's assumption. Zekri [47] did a perturbation study of gravity effect within the Wagner framework, for a body of parabolic shape, $f(x) = x^2/2R$. His analysis yields the characteristic timescale $t_g = (R\dot{h}/g^2)^{1/3}$, which is identical to Eq. (32) when taking $\beta = \sqrt{\dot{h}t_g/R}$ as the characteristic deadrise angle of the wetted parabolic contour at $t = t_g$. However, his perturbative expansion is restricted to the early stage of water impact ($t/t_g \ll 1$), when the effect of gravity can still be neglected for practical concern. Yan and Liu [48] used a boundary element method to investigate the effect of gravity during the water impact of inverted cones, with different deadrise angles. They did find that $\dot{h}/\beta gt$ could be used as a similarity parameter to describe the effect of gravity across their simulations. Defining as a Froude number, $Fr = \sqrt{\dot{h}/gt}$, their simulations predict that gravity induces a 10% increase in the impact load (hydrodynamic + hydrostatic) at $Fr \simeq 0.44; 0.98; 1.7; 2.6$ for $\beta = 15^\circ; 30^\circ; 45^\circ; 60^\circ$.

Appendix B. Computation of the Wagner wetted area

This section gives some details about the scheme implemented to solve the system of equations 9-10. The function whose root is searched for is the following:

$$G(b_1, b_2) = \begin{cases} g_1(b_1, b_2) = \int_{-b_1}^{b_2} f(x) \sqrt{\frac{b_2 - x}{b_1 + x}} dx - \frac{\pi}{2}(b_1 + b_2)h \\ g_2(b_1, b_2) = \int_{-b_1}^{b_2} f(x) \sqrt{\frac{b_1 + x}{b_2 - x}} dx - \frac{\pi}{2}(b_1 + b_2)h, \end{cases} \quad (33)$$

where h is a parameter. The root, $\Lambda = (\lambda_1, \lambda_2)$, is searched by using the Newton-Raphson method with a relaxation condition. Starting from an initial guess Λ^0 , the approximate value is iteratively improved by using the formula:

$$\Lambda^{i+1} = \Lambda^i - \omega [J_G(\Lambda^i)]^{-1} G(\Lambda^i) \quad (34)$$

where ω is a relaxation factor; $\omega = 1$ corresponds to no relaxation. J_G is the Jacobian matrix of G , given by

$$J_G = \begin{bmatrix} \frac{\partial g_1}{\partial b_1} & \frac{\partial g_1}{\partial b_2} \\ \frac{\partial g_2}{\partial b_1} & \frac{\partial g_2}{\partial b_2} \end{bmatrix}. \quad (35)$$

For some configurations, the Newton-Raphson scheme did not converge without under-relaxation. An under-relaxation factor $\omega = 0.1$ was found to provide convergence for all considered cases.

Initial guess Λ^0 . The von Karman wetted area is used as an initial guess for λ_1 and λ_2 . The von Karman solution is found by looking for the intersection points between the body contour and the initial free surface.

Stopping criterion. The iterative process is stopped when the scalar quantity

$$r(\lambda_1^i, \lambda_2^i) = \frac{\sqrt{g_1 (\lambda_1^i, \lambda_2^i)^2 + g_2 (\lambda_1^i, \lambda_2^i)^2}}{(\lambda_1^i + \lambda_2^i) h} \quad (36)$$

drops below a given threshold ε . For the results reported in the present study, the threshold was set to $\varepsilon = 10^{-4}$.

Computation of G . The body contour is approximated by a polygon. In order to reduce the discretization error for a given number of discretization points, the vertices of the polygon are uniformly distributed as a function of the variable

$$\Gamma(s) = \int |\gamma(s)| ds, \quad (37)$$

where s is the curvilinear abscissa along the body contour, and γ its curvature. The function representing the polygon, $\widehat{f}(x)$, is piecewise-linear. Making the variable substitutions

$$\xi_{\pm} = \pm[2x - (b_2 - b_1)]/(b_1 + b_2), \quad (38)$$

the integrals appearing in Eq. (33) become

$$I_-(b_1, b_2) = \int_{-b_1}^{b_2} \widehat{f}(x) \sqrt{\frac{b_2 - x}{b_1 + x}} dx = \frac{1}{2}(b_1 + b_2) \int_{-1}^1 \widehat{f}[x(\xi_-)] \sqrt{\frac{1 + \xi_-}{1 - \xi_-}} d\xi_-. \quad (39)$$

$$I_+(b_1, b_2) = \int_{-b_1}^{b_2} \widehat{f}(x) \sqrt{\frac{b_1 + x}{b_2 - x}} dx = \frac{1}{2}(b_1 + b_2) \int_{-1}^1 \widehat{f}[x(\xi_+)] \sqrt{\frac{1 + \xi_+}{1 - \xi_+}} d\xi_+ \quad (40)$$

Eq. (38) being a linear relationship between ξ_{\pm} and x , $\widehat{f}[x(\xi_+)]$ and $\widehat{f}[x(\xi_-)]$ are also piecewise-linear functions. Then, by using the antiderivatives

$$\int \sqrt{\frac{1+u}{1-u}} du = -\sqrt{1-u^2} + 2 \arcsin \sqrt{(1+u)/2} \quad (41)$$

$$\int u \sqrt{\frac{1+u}{1-u}} du = -(u/2 + 1)\sqrt{1-u^2} + \arcsin \sqrt{(1+u)/2}, \quad (42)$$

the integrals appearing in Eqs. (39-40) can be expressed as the sum of analytical terms, which are numerically added up. The partial derivatives required to compute the Jacobian matrix, J_G , are numerically obtained by using a perturbation method.

References

- [1] H. Wagner, Über sto- und gleitvorgänge an der oberfläche von flüssigkeiten, ZAMM - Journal of Applied Mathematics and Mechanics / Zeitschrift für Angewandte Mathematik und Mechanik 12 (4) (1932) 193–215. doi:10.1002/zamm.19320120402.
- [2] S. Muzaferija, M. Peric, P. Sames, T. Schellin, A two-fluid navier-stokes solver to simulate water entry, in: Proc, 22nd Symp. Naval Hydrodyn., 1998, pp. 638–651.
- [3] M. Greenhow, W.-M. Lin, Nonlinear-free surface effects: experiments and theory, Tech. rep., Massachusetts Inst. of Tech. Cambridge Dept. of Ocean Engineering (1983).
- [4] M.-C. Lin, L.-D. Shieh, Flow visualization and pressure characteristics of a cylinder for water impact, Applied Ocean Research 19 (2) (1997) 101 – 112. doi:10.1016/S0141-1187(97)00014-X.
- [5] R. Cointe, Two-dimensional water-solid impact, Journal of Offshore Mechanics and Arctic Engineering 111 (2) (1989) 109–114. doi:10.1115/1.3257083.
- [6] S. D. Howison, J. R. Ockendon, S. K. Wilson, Incompressible water-entry problems at small deadrise angles, Journal of Fluid Mechanics 222 (1991) 215–230. doi:10.1017/S0022112091001076.
- [7] M. Greenhow, Wedge entry into initially calm water, Applied Ocean Research 9 (4) (1987) 214 – 223. doi:10.1016/0141-1187(87)90003-4.
- [8] T. Tveitnes, A. Fairlie-Clarke, K. Varyani, An experimental investigation into the constant velocity water entry of wedge-shaped sections, Ocean Engineering 35 (14) (2008) 1463 – 1478. doi:10.1016/j.oceaneng.2008.06.012.
- [9] J. Wang, C. Lugni, O. M. Faltinsen, Experimental and numerical investigation of a freefall wedge vertically entering the water surface, Applied Ocean Research 51 (2015) 181 – 203. doi:10.1016/j.apor.2015.04.003.
- [10] G. V. Logvinovich, Hydrodynamics of free-boundary flows, Israel Program for Scientific Translations, 1972.
- [11] A. Tassin, A. Korobkin, M. Cooker, On analytical models of vertical water entry of a symmetric body with separation and cavity initiation, Applied Ocean Research 48 (2014) 33 – 41. doi:10.1016/j.apor.2014.07.008.
- [12] W.-Y. Duan, X. Zhu, Y. Ni, S.-J. Yu, Constant velocity water entry of finite wedge section with flow separation, J Ship Mech 17 (8) (2013) 911 [in Chinese].

- [13] R. Zhao, O. Faltinsen, J. Aarsnes, Water Entry of Arbitrary Two-Dimensional Sections with and Without Flow Separation, in: Twenty-First Symposium on Naval Hydrodynamics, 1996, pp. 408–423.
- [14] A. Iafrati, D. Battistin, Hydrodynamics of water entry in presence of flow separation from chines, in: Proceedings of the 8th International Conference on Numerical Ship Hydrodynamics, 2003, pp. 22–25.
- [15] C. Bao, G. Wu, G. Xu, Simulation of water entry of a two-dimension finite wedge with flow detachment, *Journal of Fluids and Structures* 65 (2016) 44 – 59. doi:<https://doi.org/10.1016/j.jfluidstructs.2016.05.010>.
- [16] C. Bao, G. Wu, G. Xu, Simulation of freefall water entry of a finite wedge with flow detachment, *Applied Ocean Research* 65 (2017) 262 – 278. doi:[10.1016/j.apor.2017.04.014](https://doi.org/10.1016/j.apor.2017.04.014).
- [17] K. J. Maki, D. Lee, A. W. Troesch, N. Vlahopoulos, Hydroelastic impact of a wedge-shaped body, *Ocean Engineering* 38 (4) (2011) 621 – 629. doi:[10.1016/j.oceaneng.2010.12.011](https://doi.org/10.1016/j.oceaneng.2010.12.011).
- [18] D. J. Piro, K. J. Maki, Hydroelastic analysis of bodies that enter and exit water, *Journal of Fluids and Structures* 37 (2013) 134 – 150. doi:[10.1016/j.jfluidstructs.2012.09.006](https://doi.org/10.1016/j.jfluidstructs.2012.09.006).
- [19] H. Gu, L. Qian, D. Causon, C. Mingham, P. Lin, Numerical simulation of water impact of solid bodies with vertical and oblique entries, *Ocean Engineering* 75 (2014) 128 – 137. doi:[10.1016/j.oceaneng.2013.11.021](https://doi.org/10.1016/j.oceaneng.2013.11.021).
- [20] G. Oger, M. Doring, B. Alessandrini, P. Ferrant, Two-dimensional SPH simulations of wedge water entries, *Journal of Computational Physics* 213 (2) (2006) 803 – 822. doi:[10.1016/j.jcp.2005.09.004](https://doi.org/10.1016/j.jcp.2005.09.004).
- [21] A. M. Worthington, *A study of splashes*, Longmans, Green, and Company, 1908.
- [22] C. Duez, C. Ybert, C. Clanet, L. Bocquet, Making a splash with water repellency, *Nature Physics* 3 (2007) 180–183. doi:[10.1038/nphys545](https://doi.org/10.1038/nphys545).
- [23] X. Zhu, O. M. Faltinsen, C. Hu, Water entry and exit of a horizontal circular cylinder, *Journal of Offshore Mechanics and Arctic Engineering* 129 (4) (2006) 253–264. doi:[10.1115/1.2199558](https://doi.org/10.1115/1.2199558).
- [24] H. Sun, O. M. Faltinsen, Water impact of horizontal circular cylinders and cylindrical shells, *Applied Ocean Research* 28 (5) (2006) 299 – 311. doi:[10.1016/j.apor.2007.02.002](https://doi.org/10.1016/j.apor.2007.02.002).
- [25] H. Sun, A boundary element method applied to strongly nonlinear wave-body interaction problems, Ph.D. thesis, Norwegian University of Science and Technology (2007).

- [26] A. Fairlie-Clarke, T. Tveitnes, Momentum and gravity effects during the constant velocity water entry of wedge-shaped sections, *Ocean Engineering* 35 (7) (2008) 706–716. doi:10.1016/j.oceaneng.2006.11.011.
- [27] S. Malenica, A. Korobkin, J. Tuitman, MLM_ROC modified Logvinovich model for 2D sections constant roll angle, Tech. rep., Bureau Veritas (2007).
- [28] A. Korobkin, Analytical models of water impact, *European Journal of Applied Mathematics* 15 (6) (2004) 821–838. doi:10.1017/S0956792504005765.
- [29] O. M. Faltinsen, Y. A. Semenov, Nonlinear problem of flat-plate entry into an incompressible liquid, *Journal of Fluid Mechanics* 611 (2008) 151–173. doi:10.1017/S0022112008002735.
- [30] Y. M. Scolan, E. Coche, T. Coudray, E. Fontaine, Etude analytique et numérique de l’impact hydrodynamique sur des carènes dissymétriques, in: 7e Journées de l’Hydrodynamique, 1999, pp. 151–164 [in French]. URL <http://website.ec-nantes.fr/actesjh/images/7JH/Annexe/S4P2.pdf>
- [31] R. Cointe, E. Fontaine, B. Molin, Y. M. Scolan, On energy arguments applied to the hydrodynamic impact force, *Journal of Engineering Mathematics* 48 (3) (2004) 305–319. doi:10.1023/B:engi.0000018189.83070.78.
- [32] O. M. Faltinsen, *Hydrodynamics of High-Speed Marine Vehicles*, Cambridge University Press, 2006. doi:10.1017/CB09780511546068.
- [33] R. Cointe, J.-L. Armand, Hydrodynamic impact analysis of a cylinder, *Journal of Offshore Mechanics and Arctic Engineering* 109 (3) (1987) 237–243. doi:10.1115/1.3257015.
- [34] R. Zhao, O. Faltinsen, Water entry of two-dimensional bodies, *Journal of Fluid Mechanics* 246 (1993) 593–612. doi:10.1017/S002211209300028X.
- [35] A. Korobkin, Second-order Wagner theory of wave impact, *Journal of Engineering Mathematics* 58 (1) (2007) 121–139. doi:10.1007/s10665-006-9105-7.
- [36] J. M. Oliver, Second-order Wagner theory for two-dimensional water-entry problems at small deadrise angles, *Journal of Fluid Mechanics* 572 (2007) 59–85. doi:10.1017/S002211200600276X.
- [37] A. Korobkin, S. Malenica, Modified Logvinovich model for hydrodynamic loads on asymmetric contours entering water, *International Workshop on Water Waves and Floating Bodies* (2005) 4p.
- [38] A. Tassin, N. Jacques, A. Alaoui, A. Nême, B. Leblé, Assessment and comparison of several analytical models of water impact, *The International Journal of Multiphysics* 4 (2) (2010) 125 – 140. doi:10.1260/1750-9548.4.2.125.

- [39] S. Seng, P. Pedersen, J. Jensen, Slamming and whipping analysis of ships, Ph.D. thesis, DTU Mechanical Engineering (2012).
- [40] M. Reinhard, Free elastic plate impact into water, Ph.D. thesis, University of East Anglia (2013).
- [41] A. Iafrati, A. A. Korobkin, Hydrodynamic loads during early stage of flat plate impact onto water surface, *Physics of Fluids* 20 (8) (2008) 082104. doi:10.1063/1.2970776.
- [42] I. H. Abbott, A. E. Von Doenhoff, L. Stivers Jr, Summary of airfoil data, NACA Technical Report 824 (1945) 270p.
- [43] A. A. Korobkin, V. V. Pukhnachov, Initial stage of water impact, *Annual Review of Fluid Mechanics* 20 (1) (1988) 159–185. doi:10.1146/annurev.fl.20.010188.001111.
- [44] N. Aquelet, M. Souli, L. Olovsson, Euler-Lagrange coupling with damping effects: Application to slamming problems, *Computer Methods in Applied Mechanics and Engineering* 195 (1) (2006) 110 – 132. doi:10.1016/j.cma.2005.01.010.
- [45] A. Tassin, N. Jacques, A. E. M. Alaoui, A. Nême, B. Leblé, Hydrodynamic loads during water impact of three-dimensional solids: Modelling and experiments, *Journal of Fluids and Structures* 28 (2012) 211 – 231. doi:10.1016/j.jfluidstructs.2011.06.012.
- [46] A. G. Mackie, Gravity effects in the water entry problem, *Journal of the Australian Mathematical Society* 5 (4) (1965) 427–433. doi:10.1017/S1446788700028457.
- [47] H. J. Zekri, The influence of gravity on fluid-structure impact, Ph.D. thesis, University of East Anglia (2016).
- [48] H. Yan, Y. Liu, Nonlinear computation of water impact of axisymmetric bodies, *Journal of Ship Research* 55 (1) (2011) 29–44.